



**HAL**  
open science

# Numerical study of ballast-flight caused by dropping snow/ice blocks in high-speed railways using Discontinuous Deformation Analysis (DDA)

Dong Ding, Abdellatif Ouahsine, Weixuan Xiao, Peng Du

► **To cite this version:**

Dong Ding, Abdellatif Ouahsine, Weixuan Xiao, Peng Du. Numerical study of ballast-flight caused by dropping snow/ice blocks in high-speed railways using Discontinuous Deformation Analysis (DDA). *Transportation Geotechnics*, 2020, 22, pp.100314. 10.1016/j.trgeo.2019.100314 . hal-03363776

**HAL Id: hal-03363776**

**<https://hal.utc.fr/hal-03363776>**

Submitted on 21 Jul 2022

**HAL** is a multi-disciplinary open access archive for the deposit and dissemination of scientific research documents, whether they are published or not. The documents may come from teaching and research institutions in France or abroad, or from public or private research centers.

L'archive ouverte pluridisciplinaire **HAL**, est destinée au dépôt et à la diffusion de documents scientifiques de niveau recherche, publiés ou non, émanant des établissements d'enseignement et de recherche français ou étrangers, des laboratoires publics ou privés.



Distributed under a Creative Commons Attribution - NonCommercial 4.0 International License

# Numerical study of ballast-flight caused by dropping snow / ice blocks in high-speed railways using Discontinuous Deformation Analysis (DDA)

Dong Ding<sup>a</sup>, Abdellatif Ouahsine<sup>a,\*</sup>, Weixuan Xiao<sup>a</sup>, Peng Du<sup>b</sup>

<sup>a</sup> Sorbonne Université, Université de Technologie de Compiègne  
Laboratoire Roberval

Centre de recherches Royallieu, CS 60319, 60203 Compiègne cedex, France

<sup>b</sup> School of Marine Science and Technology, Northwestern Polytechnical University, Xian 710072, China

---

## Abstract

Frozen snow / ice blocks drop at high speeds from train causing the ballast to fly up and damage the car body. Thus, in this paper, we propose a numerical model based on the discontinuous deformation analysis (DDA) method to study the ballast flight caused by dropping snow / ice blocks in high-speed railways and to analyze the dynamic behavior of ballast particles during their collision with a snow / ice block. The validation of the proposed model is done by comparing the numerical results with the theoretical and the experimental ones. The numerical results show that the velocity, shape and incident angle of snow / ice block play an important role in the ballast flight. Specifically, the number and the maximum displacement of ballast particles increase as the train speed increases and the incident angle greatly affects the movement direction of ballast particles. The shape of the ice block affects the amount and extent of ballast flight.

*Keywords:* High speed railway, ballast flight, snow-dropping, numerical modeling, discontinuous deformation analysis

---

## 1. Introduction

The phenomenon of ballast flight is one of the major problems in high speed ballasted track, which has resulted in major maintenance costs and safety concerns. Flying ballast particles may hit the rail, the train body or the passengers through stations. Furthermore, small particles of ballast may come to rest between the railhead and the wheels of rail vehicles, which cause substantial local bending damage to the rail [1]. The aerodynamic effect is commonly regarded as the main cause of ballast flight [2, 3]. However, as counted by M. R. Saat et al. [4], about 50% ballast flight incidents occur in snow condition. This is because high-speed trains run through snow zone and blow up the snow which sticks to the underfloor equipment and freezes rapidly into ice, then, the frozen snow and ice drops at high speeds from trains due to temperature changes, train vibration and heat from the brakes, causing the ballast to fly up [5, 6], as shown in Fig. 1. The effects of ballast flight caused by dropping snow/ice may lead to serious catastrophic consequences due to the high initial velocity, large mass, and chain reaction of the falling snow/ice.

Snow / ice dropping and influencing factors of ballast flight have been studied in many recent studies. Loponen *et al* [5] studied the amount of the excitation required to drop snow from the train underframe.

---

\*Corresponding author

Email addresses: [dong.ding@utc.fr](mailto:dong.ding@utc.fr) (Dong Ding), [ouahsine@utc.fr](mailto:ouahsine@utc.fr) (Abdellatif Ouahsine)

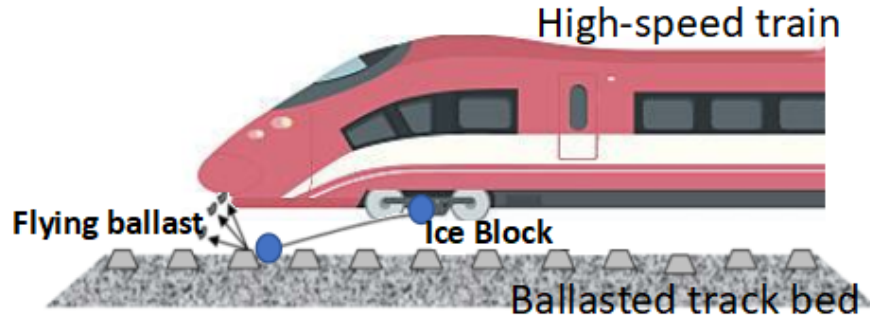


Figure 1: Schematic illustration of the mechanism and process of ballast flight caused by dropping ice block.

15 They used a simplified equilibrium equation based on the adhesive forces to indicate that the snow dropping requires an acceleration amplitude of approximately 20-2000  $g$  depending on the characteristics of the snow mass. Kawashima *et al* et al. [6] carried out an experimental study using air cannon tests to investigate the ballast-flight phenomenon caused by the dropping of accreted ice, and gave a relationship between the number of flying ballast stones and the mass, shape, speed, and angle of the ice. Furthermore, computational
 20 fluid dynamics (CFD) methods have been applied to the study of the flow between the train underbody and the track bed around the bogie area and its impact on the ballast flight [7, 8, 9]. Xie *et al* [10] used a 3-D numerical model based on the coupling between Navier-Stokes equations based model and a discrete phase model to investigate the flow field in the presence of snow accumulation in the train underframe. The numerical result showed that the snow particles accumulated and moved on the train bogies by the
 25 high-speed air. However, to the best of our knowledge, there are no computational techniques focused on the dynamic impact behavior between the ice block and the ballasted track bed which is the key reason resulting in the ballast flight during winter. In this study, the discontinuous deformation analysis (DDA) method is used to determine the displacement of irregular ballast particles and the collision between ice block and ballast particles. DDA is a kind of discrete element method (DEM), developed by G.H. Shi in
 30 1989 for application of rock fracture mechanics and geotechnical or structural problems [11, 12]. Ishikawa T. et al. first used DDA for simulating deformation behavior of ballast [13], which showed good performance in the study of coarse granular materials.

The main purpose of this paper is to determine the influence factors of ballast flight and to analyze the dynamic behavior of ballast particles during their collision with a snow / ice block. In the DDA method,
 35 the kinematic conditions of the contact surfaces are enforced through the penalty method in order to avoid the inter-penetration between blocks. The performance of the ballast flight is evaluated by considering the velocity, the shape and the incident angle of snow / ice blocks. The numerical results show that these factors influence significantly the ballast particles dynamics and also their flight as well as the collision between ballast particles.

## 40 2. Theoretical background and governing equations

As the computation domain is composed of discrete elements, we use the Discontinuous Deformation Analysis (DDA) method which is based on the principle of minimum potential energy. The DDA method does not have the meshing procedure of blocks and therefore, no refinement is needed to improve the quality of the calculated solution, which has the advantage of reducing the computation time [14, 15].

45 In the DDA method, the displacement  $(u, v)$  at any point  $(x, y)$  of a block  $i$  can be represented by six variables: two translations ( $u_c, v_c$ ) of the block gravity center  $(x_c, y_c)$  in x and y directions, a rotation  $\gamma_c$  around  $(x_c, y_c)$ , and two normal and a shear strains ( $\varepsilon_{xx}, \varepsilon_{yy}, \varepsilon_{xy}$ ); therefore, the variables vector associated with the block  $i$  is given:

$$\mathbf{D}_i = \left( u_c, v_c, \gamma_c, \varepsilon_{xx}, \varepsilon_{yy}, \varepsilon_{xy} \right)^T \quad (1)$$

According to the first-order expression of any point  $(x, y)$ , the displacement  $(u, v)$  for an individual block  
50  $i$  can be written as:

$$\mathbf{U}_i = \begin{pmatrix} u \\ v \end{pmatrix} = \mathbf{T}_i \mathbf{D}_i \quad (2)$$

where

$$\mathbf{T}_i = \begin{pmatrix} 1 & 0 & -(y - y_c) & (x - x_c) & 0 & (y - y_c)/2 \\ 0 & 1 & (x - x_c) & 0 & (y - y_c) & (x - x_c)/2 \end{pmatrix} \quad (3)$$

The strain of the block  $i$  can be expressed by the relationship between the strain and displacement:

$$\boldsymbol{\varepsilon}_i = \mathbf{L} \mathbf{U}_i \quad (4)$$

Where  $\mathbf{L} = \begin{pmatrix} \frac{\partial}{\partial x} & 0 \\ 0 & \frac{\partial}{\partial y} \\ \frac{1}{2} \frac{\partial}{\partial y} & \frac{1}{2} \frac{\partial}{\partial x} \end{pmatrix}$  is the differential operator matrix for 2D problem.

55 Substituting Eq. (2) into Eq. (4), we get:

$$\boldsymbol{\varepsilon}_i = \mathbf{L} \mathbf{T}_i \mathbf{D}_i = \mathbf{B} \mathbf{D}_i \quad (5)$$

Assuming that the deformation is elastic and linear, the stress tensor is written as follows:

$$\boldsymbol{\sigma}_i = \mathbf{E} \boldsymbol{\varepsilon}_i = \mathbf{E} \mathbf{B} \mathbf{D}_i \quad (6)$$

Where  $\mathbf{E}$  is the elastic matrix of deformation planes and  $\mathbf{B} = \begin{bmatrix} 0 & 0 & 0 & 1 & 0 & 0 \\ 0 & 0 & 0 & 0 & 1 & 0 \\ 0 & 0 & 0 & 0 & 0 & 1 \end{bmatrix}$ .

The total potential energy  $\Pi_p$  of the block  $i$ , defined as the the sum of the elastic strain energy  $\Pi_e$ , initial  
60 stress potential energy  $\Pi_{\sigma_0}$ , body force potential energy  $\Pi_b$ , and inertial energy  $\Pi_i$ , is given by:

$$\begin{aligned} \Pi_p &= \sum \Pi = \Pi_e + \Pi_{\sigma_0} + \Pi_b + \Pi_i \\ &= \int_{A_i} \frac{1}{2} \boldsymbol{\varepsilon}_i^T \boldsymbol{\sigma}_i dA_i + \int_{A_i} \boldsymbol{\varepsilon}_i^T \boldsymbol{\sigma}_0 dA_i - \int_{A_i} \mathbf{U}_i^T \mathbf{f}_b dA_i + \int_{A_i} \mathbf{U}_i^T m \ddot{\mathbf{D}}_i dA_i \end{aligned} \quad (7)$$

By using Eq.(2), it follows:

$$\Pi_p = \int_{A_i} \frac{1}{2} \boldsymbol{\varepsilon}_i^T \mathbf{E} \boldsymbol{\varepsilon}_i dA_i + \int_{A_i} \boldsymbol{\varepsilon}_i^T \boldsymbol{\sigma}_0 dA_i - \mathbf{D}_i^T \mathbf{T}_i^T \left( \int_{A_i} \mathbf{f}_b dA_i - \int_{A_i} m \mathbf{T}_i \ddot{\mathbf{D}}_i dA_i \right) \quad (8)$$

where  $\mathbf{f}_b$  denotes the body forces applied on a block  $i$ , and  $m$  is the block mass per unit area.  $\boldsymbol{\sigma}_0$  is the initial stress of the block.

Substituting Eq. (5) and (6) into Eq. (8), the total potential of a system of  $N$  blocks is expressed as:

$$\Pi_{np} = \sum_1^N \left( \mathbf{D}_i^T \mathbf{M} \ddot{\mathbf{D}}_i + \frac{1}{2} \mathbf{D}_i^T \mathbf{K} \mathbf{D}_i - \mathbf{D}_i^T \mathbf{f}_e \right) \quad (9)$$

where  $\mathbf{M} = \int_{A_i} m \mathbf{T}_i^T \mathbf{T}_i dA_i$  is the mass matrix,  $\mathbf{K} = \int_{A_i} \mathbf{B}^T \mathbf{E} \mathbf{B} dA_i$  is the stiffness matrix,  $\mathbf{f}_e = \int_{A_i} (\mathbf{T}_i^T \mathbf{f}_b - \mathbf{B}^T \boldsymbol{\sigma}_0) dA_i$  is the external forces matrix. According to the minimized potential energy, the block system equations of motion can be represented in the compact form:

$$\frac{\partial \Pi_p}{\partial \mathbf{D}_i} = 0 \Rightarrow \mathbf{M} \ddot{\mathbf{D}} + \mathbf{K} \mathbf{D} = \mathbf{F} \quad (10)$$

Using the Newmark- $\beta$  method to solve the kinematic equation of motion Eq. (10), the displacement and velocity can be approximated as:

$$\begin{aligned} \mathbf{D}_{n+1} &= \mathbf{D}_n + \Delta t \dot{\mathbf{D}}_n + \frac{\Delta t^2}{2} \left[ (1 - 2\beta) \ddot{\mathbf{D}}_n + 2\beta \ddot{\mathbf{D}}_{n+1} \right] \\ \dot{\mathbf{D}}_{n+1} &= \dot{\mathbf{D}}_n + \Delta t \left[ (1 - \gamma) \ddot{\mathbf{D}}_n + \gamma \ddot{\mathbf{D}}_{n+1} \right] \end{aligned} \quad (11)$$

where  $\ddot{\mathbf{D}}$  and  $\dot{\mathbf{D}}$  are the acceleration and the initial matrix of each time step, while  $\beta$  and  $\gamma$  are velocity and acceleration weighting parameters respectively. Specifications for  $\beta$  and  $\gamma$  parameters lead to various time integration schemes. In the present investigation, we assume that  $\beta = 1/2$  and  $\gamma = 1$ , which is an implicit scheme that gives a stable and accurate computed solution [16, 17, 18]. Substituting Eq. (11) into Eq. (10), we get the equations of motion:

$$\left( \mathbf{K} + \frac{2\mathbf{M}}{\Delta t^2} \right) \mathbf{D}_{n+1} = \mathbf{F} + \frac{2\mathbf{M}}{\Delta t} \dot{\mathbf{D}}_n \quad (12)$$

The final motion equations can be written in compact form as:

$$\hat{\mathbf{K}} \mathbf{D} = \hat{\mathbf{F}} \quad (13)$$

where  $\hat{\mathbf{K}} = \frac{2\mathbf{M}}{\Delta t^2} + \mathbf{K}$ , and  $\hat{\mathbf{F}} = \mathbf{F} + \frac{2\mathbf{M}}{\Delta t} \dot{\mathbf{D}}_n$ . Note that in the present study we used an implicit scheme, thus the explicit damping is assumed to be zero. Furthermore, the DDA method is used in both static and dynamic analyses. The only difference is that in static calculations, the velocity at the beginning of each time step is assumed to be zero, while the dynamic calculation inherits the velocity of the previous time step which is contributed by the inertia force.

At every time steps, the simultaneous equilibrium of  $N$  blocks Eq. (13) can be written as:

$$\begin{pmatrix} \mathbf{K}_{11} & \mathbf{K}_{12} & \mathbf{K}_{13} & \cdots & \mathbf{K}_{1n} \\ \mathbf{K}_{21} & \mathbf{K}_{22} & \mathbf{K}_{23} & \cdots & \mathbf{K}_{2n} \\ \mathbf{K}_{31} & \mathbf{K}_{32} & \mathbf{K}_{33} & \cdots & \mathbf{K}_{3n} \\ \vdots & \vdots & \vdots & \vdots & \vdots \\ \mathbf{K}_{n1} & \mathbf{K}_{n2} & \mathbf{K}_{n3} & \cdots & \mathbf{K}_{nn} \end{pmatrix} \begin{pmatrix} \mathbf{D}_1 \\ \mathbf{D}_2 \\ \mathbf{D}_3 \\ \vdots \\ \mathbf{D}_n \end{pmatrix} = \begin{pmatrix} \mathbf{F}_1 \\ \mathbf{F}_2 \\ \mathbf{F}_3 \\ \vdots \\ \mathbf{F}_n \end{pmatrix} \quad (14)$$

where  $F_i$  and  $D_i$  are the  $6 \times 1$  matrices of forces and displacements of block  $i$ . The stiffness sub-matrices  $K_{ij}$  can be explained by the example as shown in Fig. 2. There are three blocks which have two contacts: (Block 1, Block 2) and (Block 1, Block3), as shown in Fig. 2(a), the stiffness sub-matrices of the three blocks  $K_{ij}(i, j = 1, 2, 3)$  as indicated in Fig. 2(b), where the gray diagonal partitions are contributed by deformation of block  $i$ , while the other parts are derived from contact springs. Because there are no contact between Block 2 and 3, the contact stiffness sub-matrix  $K_{23}=K_{32}=0$ .

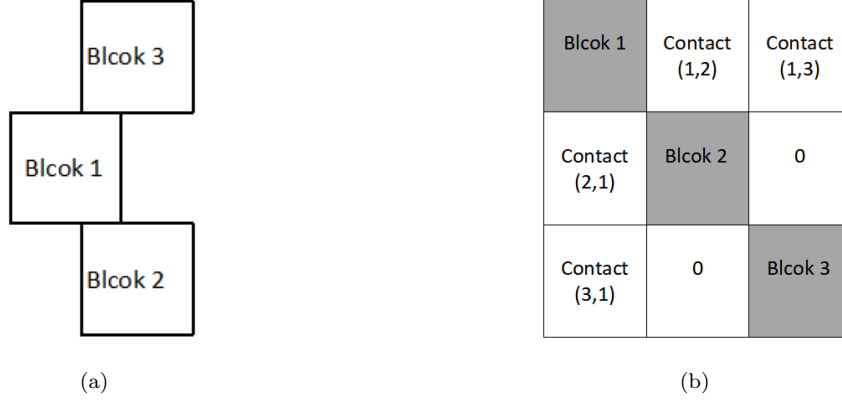


Figure 2: The structure of stiffness matrix in the case of three blocks:(a) Location of three blocks; (b) Structure of stiffness matrix

Thereafter, it should be noted that in the present investigations, in order to get the contact springs between blocks and avoid inter-penetration between blocks, the surface contact constraints are enforced by the penalty method [19], which is equivalent to placing a spring between the two blocks, by considering the contact of two blocks  $i$  and  $j$ , the penetration distance  $\delta$ , of point  $P_1$  into edge  $P_2P_3$  of block  $j$ , as shown in Fig. 3.

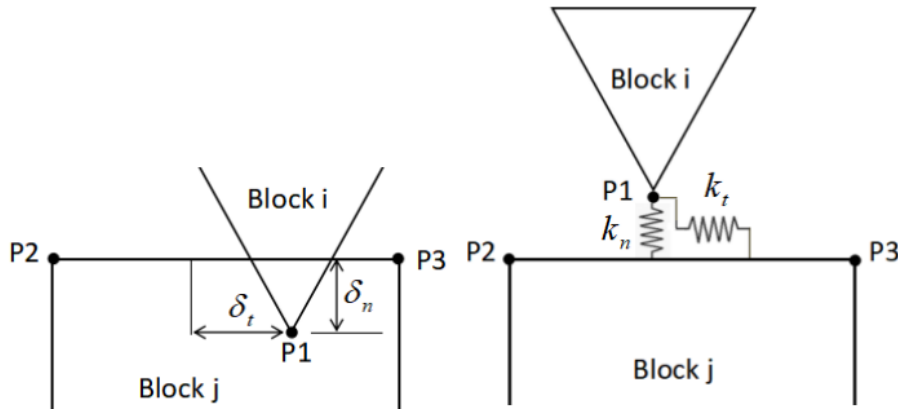


Figure 3: Interaction between two contacting blocks

This method does not increase the number of governing equations and the solution can easily be obtained by adding a contact sub-matrix to the stiffness matrix [12, 20]. The strain energy of the contact spring is:

$$\Pi_c = \frac{1}{2}k_n\delta_n^2 + \frac{1}{2}k_t\delta_t^2 \quad (15)$$

where  $k_n$  and  $k_t$  are the normal and tangential stiffness, while  $\delta_n$  and  $\delta_t$  are the penetration overlap in

normal and tangential direction. The contact strain energy should also be minimized; therefore, the penalty number  $k_n$  and  $k_t$  are assumed to be large, which can achieve an accurate result.

### 3. Validation of the DDA method

#### 3.1. Case1: Frictionless impact - Free fall

100 In order to examine the accuracy of impact in DDA, the progress of free fall and elastic rebound was simulated. The simulation consisted of  $1\text{ m} \times 1\text{ m}$  block falling  $5.0\text{ m}$  onto a  $1\text{ m} \times 10\text{ m}$  base block with four fixed points, as shown in Fig. 4(a). We have an initial velocity of  $0\text{ m/s}$ , and we assume an acceleration due to the gravity of  $10\text{ m/s}^2$ . The velocity of fall and rebound can be written as:

$$\begin{cases} V_{fall} = V_0 + gt & 0 \leq t \leq 1 \\ V_{rebound} = V_t - gt & 1 < t \leq \frac{V_t}{g} \end{cases} \quad (16)$$

105 where  $V_{fall}$  and  $V_{rebound}$  are the velocity during the fall and rebound.  $V_t$  is the velocity when the block reaches the impact plane.

The velocity of free fall and rebound for four various contact stiffness values was simulated using the DDA method. The theoretical value of free fall and elastic rebound velocity after the frictionless impact was calculated by Eq. (16). and the numerical results are shown in Fig. 4(b), where we assume that the contact stiffness is related to the Young modulus of block material [21]. The results (Fig. 4(b)) show that 110 the greater the contact stiffness is, the less the impact damping will be. It shows that the best agreement between theoretical and numerical results is met when the contact stiffness value is around  $10^9\text{ N/m}$ . It is worth noting that for smaller contact stiffness, the penetration overlap is large and then the impact between blocks becomes inelastic.

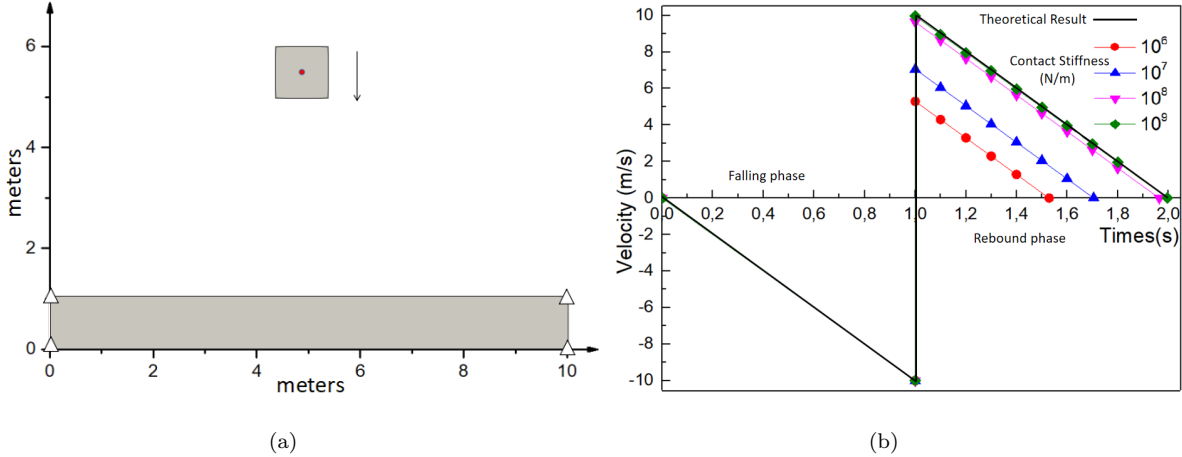


Figure 4: Falling block for testing frictionless impact and elastic rebound:(a) Schematic diagram of free fall motion; (b) Comparison between the theoretical value (Eq. (16)) and DDA results for different contact stiffness

#### 3.2. Case2: Dynamic behavior of ballast bed after collision. Comparison with experimental results

115 In this second test, the dynamic behavior of ballasted track bed at the time of collision with an ice block was verified according to the air cannon experimental results by KawashimaI et al [6]. The behavior of a

600 mm × 105 mm ice block with a velocity of 80 km/h was simulated, and the computed results were compared with the experimental observations. The DDA simulations exhibited phenomenon of ballast flight similar to the ones observed experimentally, as shown in Fig. 5. The number of ballast particles thrown 330

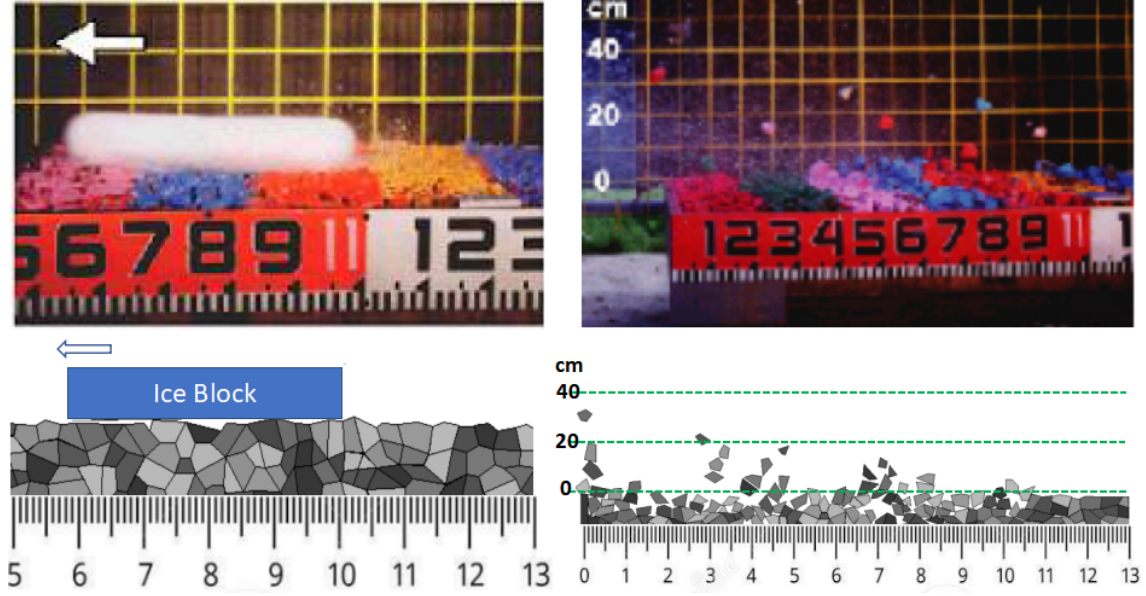


Figure 5: Comparison between the numerical and experimental responses [6] of the blocks for the DDA method.

120 mm (distance from the ballast to the train underframe) or higher  $N_{33}$  for two different mass was calculated by the current DDA model. Due to the shape of the ice block in the air cannon test is cylindrical, its mass can be calculated by:

$$M_{ice} = \rho\pi\left(\frac{d}{2}\right)^2 H \quad (17)$$

where  $\rho = 0.9340 \times 10^{-6} kg/mm^3$  is the density of ice [22], and  $d = 105 mm$  is the diameter of the cylinder. The mass of the ice block depends on the height of the ice cylinder  $H$ . The results from both experimental and numerical simulations showed that the number of the flying ballast particles increases as the velocity and the mass of ice block increase, as shown in Fig. 6. The numerical results agree well with the experimental results.

## 4. Simulation results

### 4.1. Velocity of ice block

#### 130 4.1.1. Cross section

The ballast shoulder has a width of 500 mm and a height of 100 mm, whereas the ballast bed has a thickness of 350 mm (see Fig. 7). Based on the European standard: *aggregates for railway ballast (13450, 2002)* [23], the gradation of ballast particles is from 31.5 mm to 63 mm, where the ballast particles have an irregular shape and are completely compacted. The ice block is assumed to be a circular shape with a diameter of 100 mm, which falls from a height of 600 mm on the ballast bed, where the falling distance is approximately equal to the height of the rail plus half of the height of the bogie. Adding the unit mass,

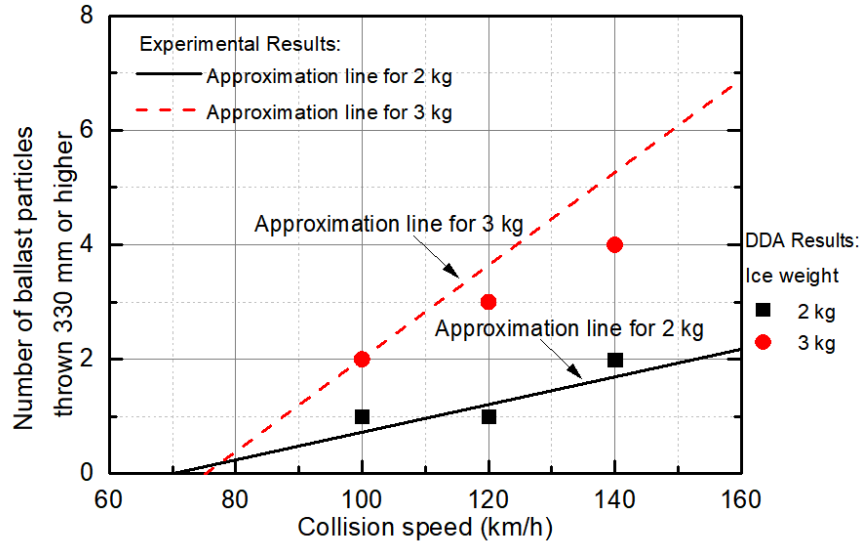


Figure 6: Comparison between the numerical and experimental values of  $N_{33}$  [6] for the DDA.

elastic modulus, Poisson ratio, friction angle, etc. to the stiffness matrix in accordance to the physical characteristics of the ballast and the ice [22, 24], as shown in Table 1.

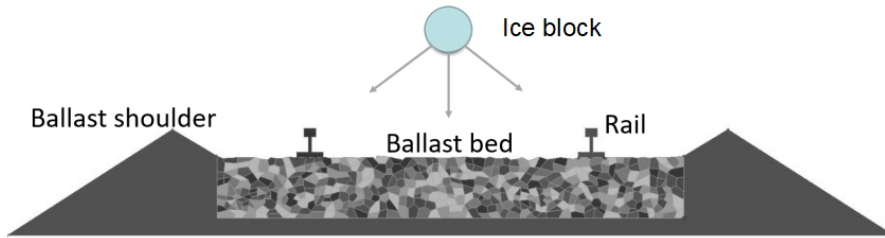


Figure 7: Track bed model

Table 1: The material parameters of ice and ballast

	Unit mass	Elastic modulus	Poisson ratio	Friction angle
Ice	$934kg/m^3$	$10GPa$	0.06	–
Ballast	$2600kg/m^3$	$50GPa$	0.20	$45^\circ$

The initial vertical velocity is related to the falling location. In addition to the bogie position, ice and snow may also pack and fall off in the coupler pocket, on the top of the train, at the train connection, or even on the overhead contact system (OCS). The standard height of contact wire is 5.1 m from the top of the rail [25], and the initial vertical velocity of falling ice from OCS is about 10 m/s. Therefore, in the present numerical investigations, we used 0 m/s, 5 m/s and 10 m/s as initial vertical velocities. Overall, the simulation results presented below show that ballast flight responses to increased velocity varied significantly. There are three key phenomena, are shown in Fig. 8: (1) the movement trajectory of the ice block; (2) the evolution of the marked ballast displacement; and (3) the responses of the ballast bed. The phenomenon

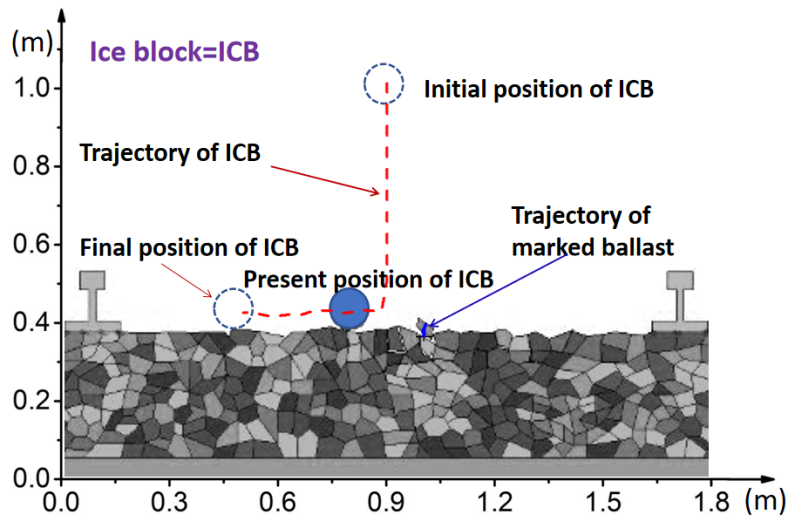
shows that the ice block after the collision first rebounded and then rolled. The displacement of ice block increases with the initial vertical velocity. When the vertical velocity exceeds  $5\text{ m/s}$ , the ice block hits the rail, or even bounce and a secondary strike on the track bed happens when the velocity is more than  $10\text{ m/s}$ . For the ballast after the collision, the higher the initial vertical velocity, the higher rebound of marked ballast is ejected, the severity of ballast bed responses is generated, and the greater the number of ballast particles is ejected. From Fig. 9, we can get the same results, the number of flying ballasts and flying height of the ballast increase with the initial vertical velocity.

Fig. 10 shows the displacement of the ice block and a marked ballast. In general, larger initial velocity induces greater displacement. However, unlike in the case of small and moderate initial vertical velocities ( $0\text{ m/s}$  and  $5\text{ m/s}$ ), during the collision process at initial vertical velocity of  $10\text{ m/s}$ , there is a collision between ice block and rail, which may reduce significantly the displacement of ice block after the impact (see Fig.10a). It follows that the ballast trajectories and displacement show that its movement may be divided into three phases. Taking the initial vertical velocity of  $5\text{ m/s}$  as an example (see Fig. 10(b)), the first phase sited between  $t= 0\text{ s}$  and  $t= 0.11\text{ s}$  corresponds to a stable state of the ballast which remains motionless before its impact by the ice blocks. The second phase sited between  $t= 0.11\text{ s}$  and  $t= 0.34\text{ s}$  corresponds to the impact and flying processes in which the ballast undergoes a rebound following a parabolic curve. The third phase sited after  $t= 0.34\text{ s}$  corresponds to the marked ballast fly-back. It should be mentioned that the severity and the duration of every phase strongly depend on the initial vertical velocity. The increased initial vertical velocity induces greater displacement of the ballast, and longer flight duration, which results in a more serious consequence.

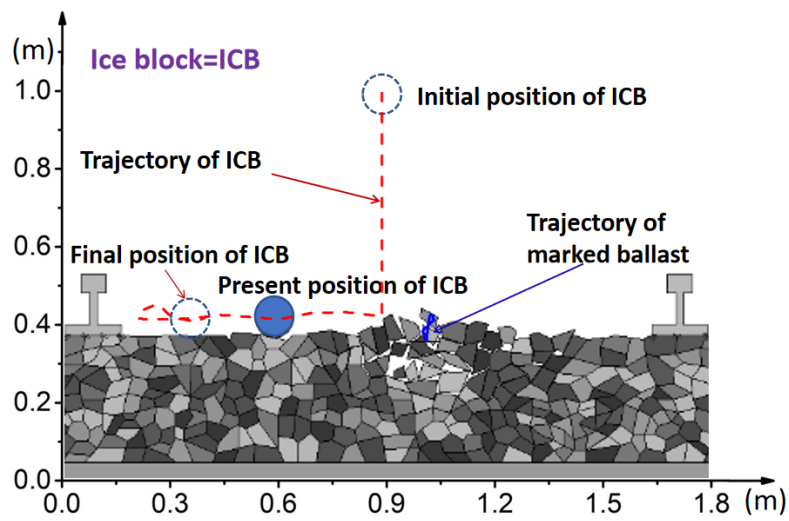
#### 4.1.2. Longitudinal section

The longitudinal section is more realistic since it considers the real velocity of the ice block dropping from high-speed trains. The high-speed railway is commonly defined by the maximum running speed exceeds  $200\text{ km/h}$ . However, the running speed of high-speed railways in China, Japan and France exceeds  $300\text{ km/h}$  and even the maximum test speed of the eastern line in France is  $574.8\text{ km/h}$  [26]. In addition, many ultra-high-speed railways are under development and under construction. In order to analyze the initial dropping velocity of the ice block, the initial collision position was set on the surface of the ballast bed. An initial vertical velocity of  $3.5\text{ m/s}$  which corresponded to the falling height of  $600\text{ mm}$ , the initial longitudinal velocity equal to the train running speed, and four initial longitudinal velocities from  $100\text{ km/h}$  to  $400\text{ km/h}$  with an interval of  $100\text{ km/h}$  were used.

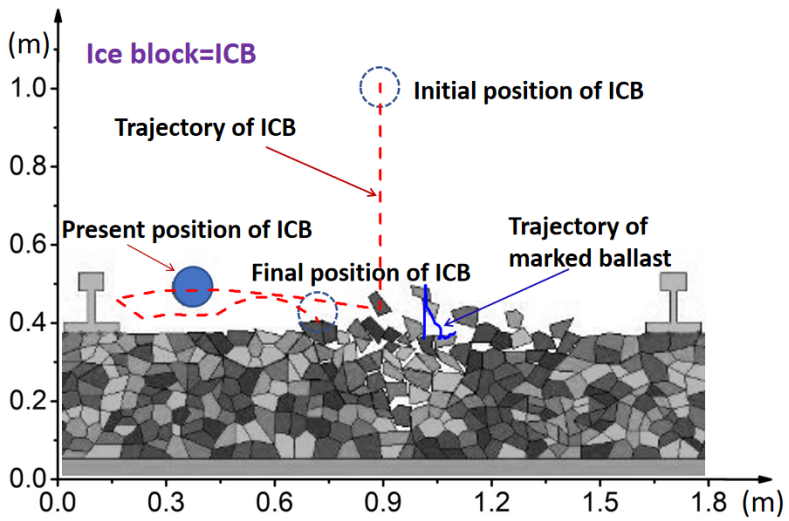
The trajectory of the ice block and marked ballast, as well as the phenomenon of ballast bed after collision, is represented in Fig. 11. It is clear that the track bed was damaged after the collision, the ballast particles were hit and displaced, and the surface of the track bed showed different degrees of depression. The severity of the damage of the track bed had a positive relationship with the initial longitudinal velocity. For the trajectory of the ice block, the ice block quickly flew upward and forward after the collision. For the trajectory of marked ballast, we know that the ballast flew to the front direction. The height and distance of the ballast flight increased with the initial longitudinal velocity. When the dropping longitudinal velocity is more than  $300\text{ km/h}$ , the marked ballast may collide with the train underframe since the maximum



(a)



(b)



(c)

Figure 8: Computed ballast flight depending on the initial vertical velocity: (a)  $V_y = 0 \text{ m/s}$  (free fall); (b)  $V_y = 5 \text{ m/s}$ ; (c)  $V_y = 10 \text{ m/s}$

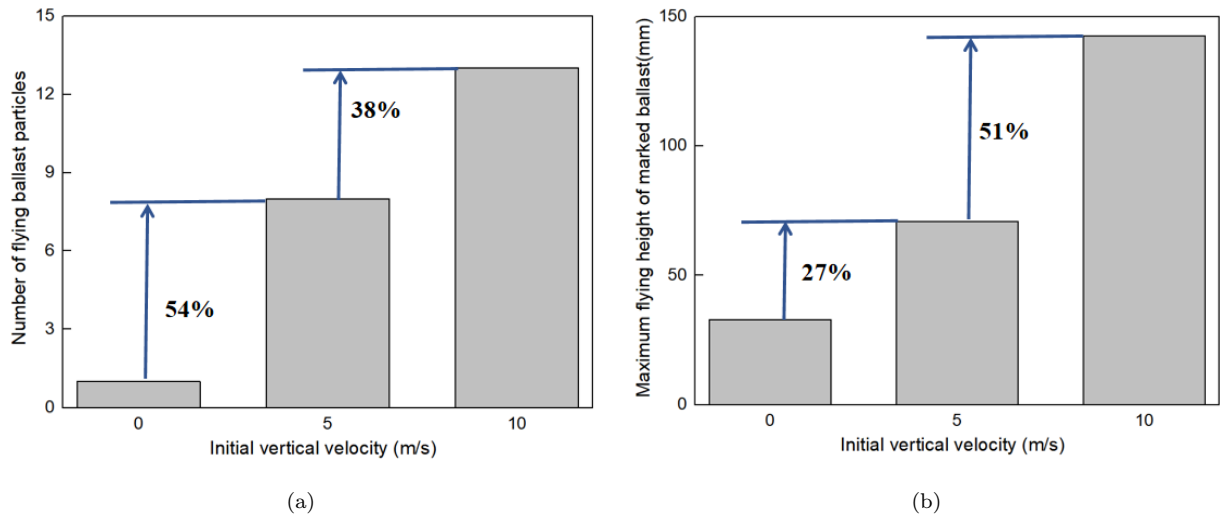


Figure 9: Relationship between (a) number of flying ballast particles and initial vertical velocity of ice block; (b) maximum flying height and initial vertical velocity of ice block

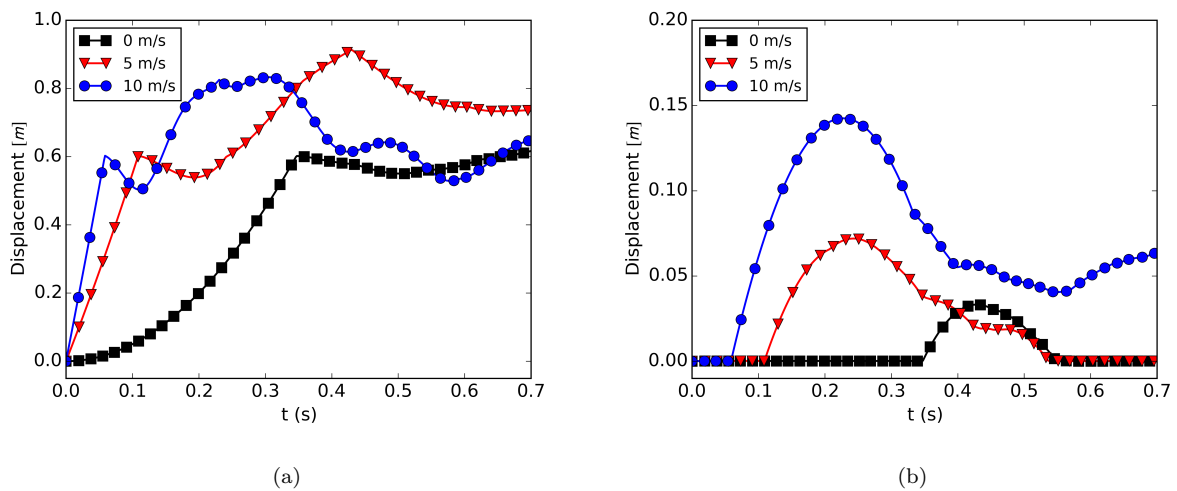


Figure 10: The displacement of (a) ice block and (b) marked ballast for different initial vertical velocity in cross section

185 height of the marked ballast after the collision is more than 330 mm (distance from the ballast bed to train underframe)[6]. If the ice and ballast particles reach the train underframe, they may accelerate significantly due to the collision with the train or may strike off more ice /snow blocks, causing more serious consequences. Indeed, the effects of ballast projection may vary from depend on where the particle lands. By considering the ballast particles flying height  $H$ , the impact risk is classified into three categories:

- 190
- If  $H \leq 184$  mm (height of UIC-60 rail), flying ballast particles have the possibility to hit the rail;
  - If  $184$  mm  $< H \leq 330$  mm, flying ballast particles have the possibility to hit the wheels of the train ;
  - If  $H > 330$  mm, flying ballast particles will certainly hit the bottom of the train, and probably the rail and the wheels of the train.

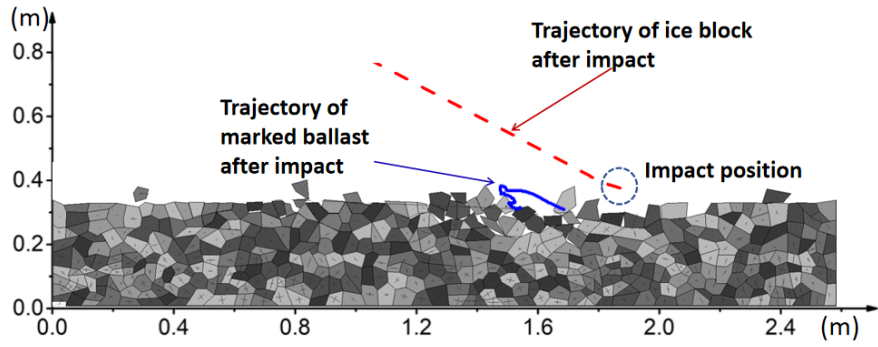
The displacement of the marked ballast and the ice block was calculated, as shown in Fig. 12. Results 195 show that the displacement of marked ballast is linear with increasing initial longitudinal velocity at  $t=0.5$  s. The displacement of marked ballast of 400 km/h is about four times of that 100 km/h. Significantly, the initial longitudinal velocity of the ice block directly affects the displacement of ice block and ballast particles. From Fig. 13, the numerical results show that the number of flying ballast particles and the vertical displacement of marked ballast increases from 100 km/h to 400 km/h. When the longitudinal 200 velocity of ice block is in the range of 200 km/h to 300 km/h, the results exhibit a peak of 33 % and 47 % of the total number of flying ballast and maximum flying height of marked ballast. Above 300 km/h, this process evolution increases gradually until a plateau is reached. This non-uniform evolution may be related to the gradation of ballast composed of different particle sizes. As the longitudinal velocity increases, most of the small size and a part of the middle size of ballast particles in the impacted area fly above the bed 205 surface.

According to the above simulation results, the initial longitudinal velocity of the snow / ice block which is directly dependent on the running speed of the train, has a great impact on the ballast flight. Reducing the speed of trains is the simplest and most effective mitigation strategy. However, this method may defeat the main purpose of high-speed lines. The national center of operation of SNCF in France proposed a time 210 schedule which divided train speed into three kinds: acceptable, tolerable and unacceptable. The weather forecast, mechanical simulation, and safety approach were taken into consideration.

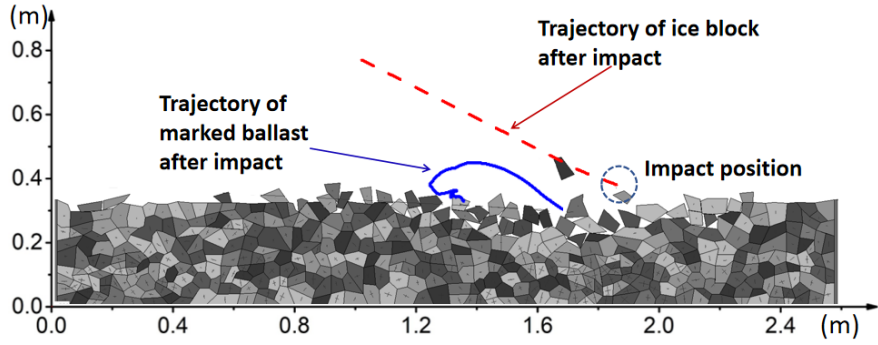
#### 4.2. Incident angle of ice/snow

Regarding the angle of incidence of the ice block, in the longitudinal section, this angle can correspond to different attachment position of the ice, as shown in Fig. 14. The incident angle is not an independent 215 variable, while it is related to the train speed and the distance of drop as well as the ice dropping position; therefore, four angles ( $0^\circ$ ,  $30^\circ$ ,  $60^\circ$ , and  $90^\circ$ ) were investigated in the simulation. The incident angles were controlled by the velocity of the longitudinal and vertical directions. The total velocity was set to 20 m/s.

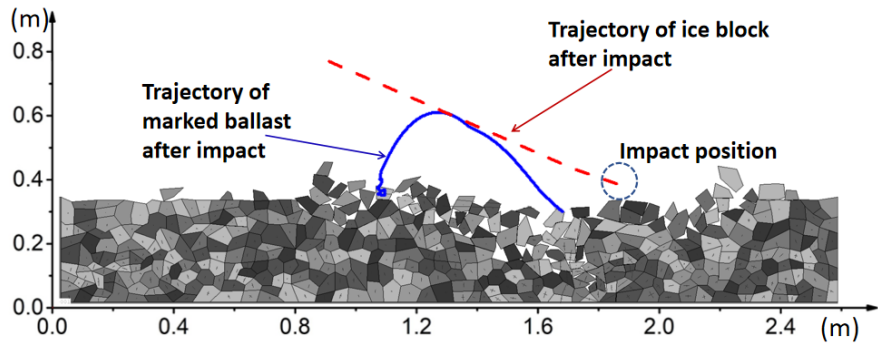
Fig. 15 shows the trajectory of the ice block and the marked ballast as well as the response of the track bed after the collision at different ejection angles. Based on these simulation results, it can be seen that 220 the incident angle is also one of the main factors affecting ballast flight. When the incident angle is  $0^\circ$ , the



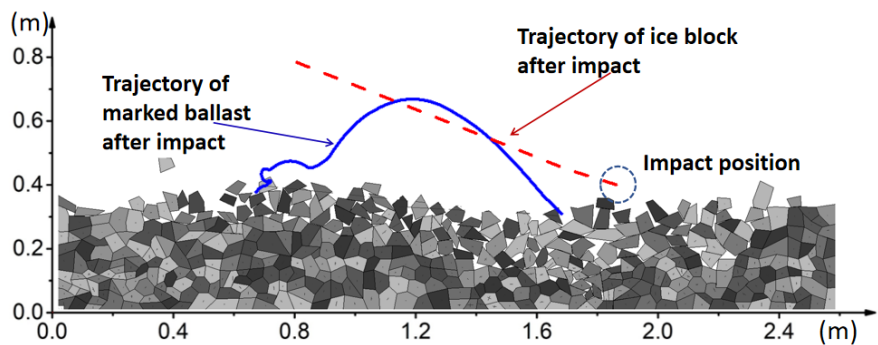
(a)



(b)



(c)



(d)

Figure 11: Relationship between ballast flight and longitudinal velocity: (a)  $V_x=100\text{ km/h}$ ; (b)  $V_x=200\text{ km/h}$ ; (c)  $V_x=300\text{ km/h}$ ; (d)  $V_x=400\text{ km/h}$

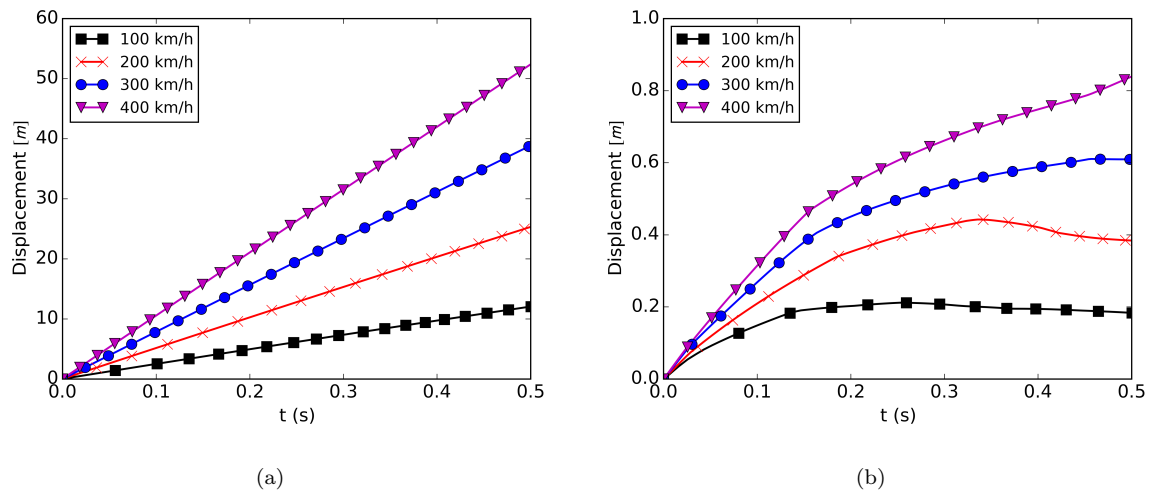


Figure 12: The displacement of (a) ice block and (b) marked ballast for different velocities in longitudinal section

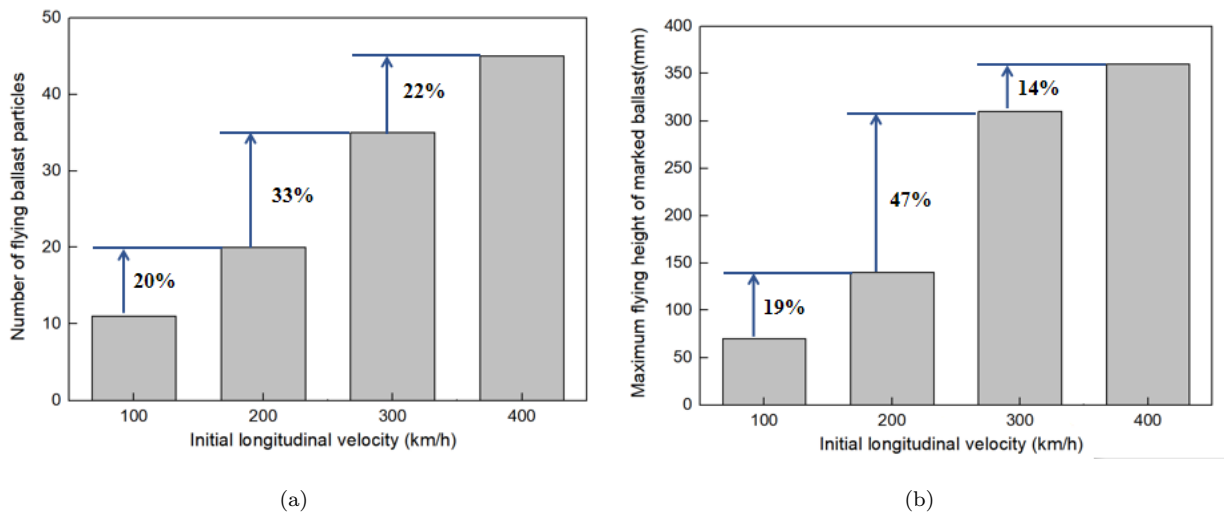


Figure 13: Relationship between (a) number of flying ballast particles and initial longitudinal velocity of ice block; (b) maximum flying height and initial longitudinal velocity of ice block

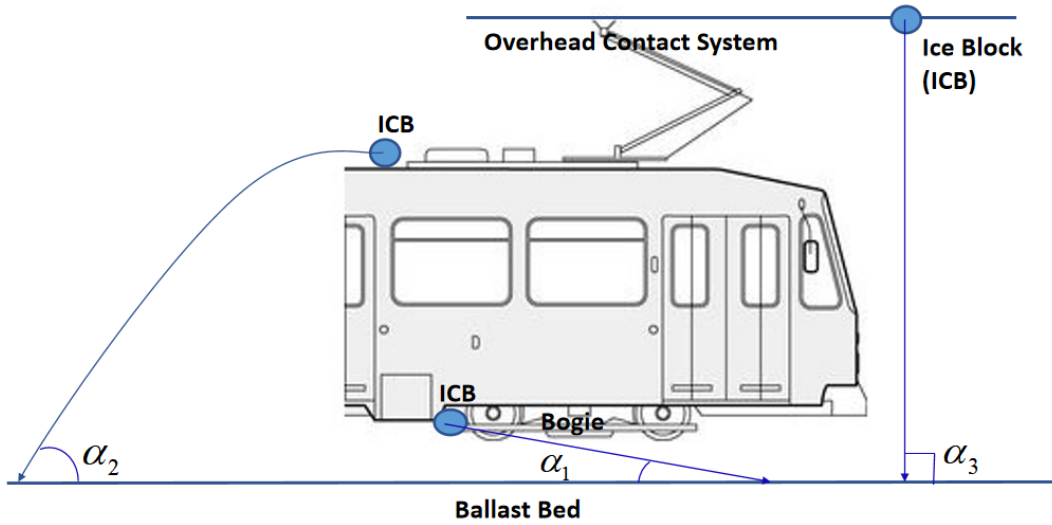


Figure 14: Three ice dropping types and incident angles

effect is insignificant, and just two ballast particles are moved above the surface. The maximum vertical displacement of the marked ballast is only 1.1 *cm*. Among the four angles, the ejection angle of  $90^\circ$  has the widest and the deepest impact, where the displacement direction of the marked ballast is essentially vertical. When the angle is  $30^\circ$  or  $60^\circ$ , there is a larger longitudinal and vertical displacement. Comparing  
 225 the reflection angles of the ice block in the four cases, the larger the angle of incidence, the larger the angle of reflection, and the greater the probability that the ice block collides with the bottom of the train. Fig. 16 shows the displacement of the ice block and the marked ballast. The ice block with the incident angle of  $0^\circ$  has the largest displacement of the four angles since the velocity in the longitudinal direction is larger than the others. However, for the displacement of the marked ballast, the displacement of the ballast with  
 230 an incident angle of  $0^\circ$  is the smallest. The displacement at incident angle of  $30^\circ$  and  $60^\circ$  is larger than the other two. Furthermore, the marked ballast of  $90^\circ$  has a large second rebound process (see Fig. 15(d) and 16(b)).

#### 4.3. Shape of ice block

In the third simulation, circular, triangular and square ice blocks with a diameter/side length of 100  
 235 *mm* were placed 600 *mm* above the ballast bed surface at the center of the track. With the initial vertical velocity of 10 *m/s*, the impact results are shown in Fig. 17.

Three shapes of ice block trajectories are significantly different. The triangular ice intrudes the ballast bed directly after colliding, while the square ice bounces off. The trajectory of the circular bounced and hit the trackbed twice. Furthermore, according to the response of the ballast bed after collision, the triangular  
 240 ice ejected the greatest number of particles and caused the greatest height of ejection, on account of its contact area with the track bed being the smallest, resulting in maximum pressure. The square ice has the widest and the deepest impact among the three, due to its larger contact area and greater mass. The results of the displacement of the ice block and the marked ballast are shown in Fig. 18. After the collision, the triangular ice has the smallest displacement and the square ice has the largest rebound. The triangular ice

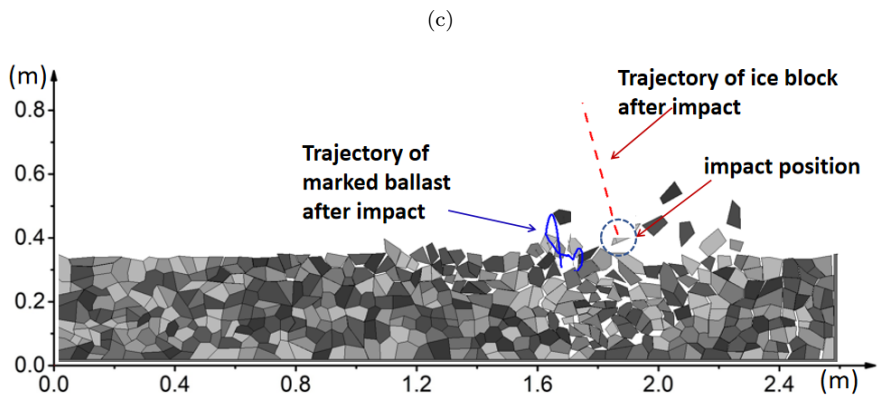
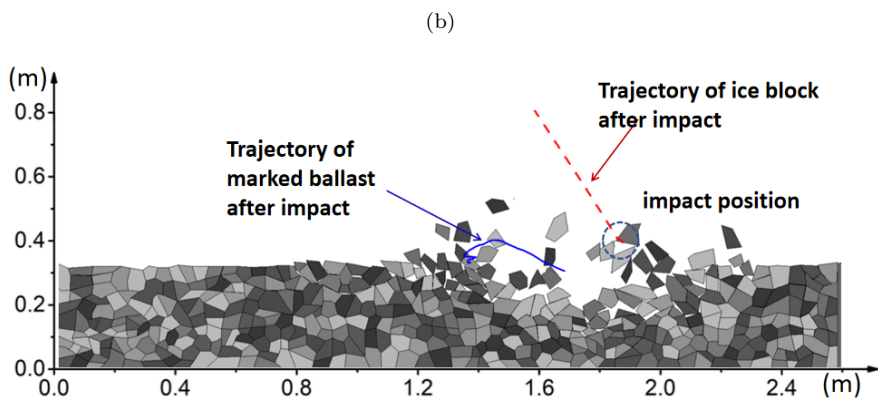
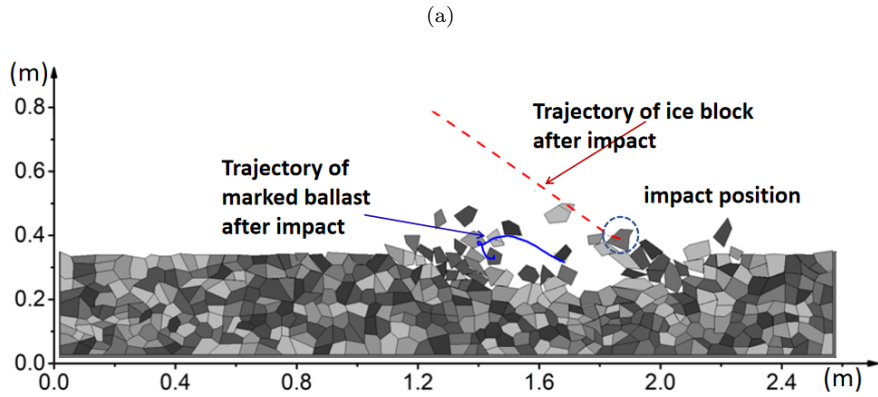
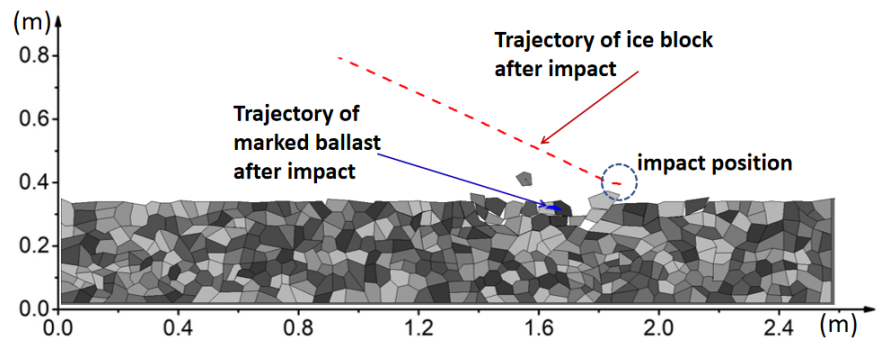


Figure 15: Ballast flight at different incident ejection angles: (a)  $\alpha = 0^\circ$ ; (b)  $\alpha = 30^\circ$ ; (c)  $\alpha = 60^\circ$ ; (d)  $\alpha = 90^\circ$

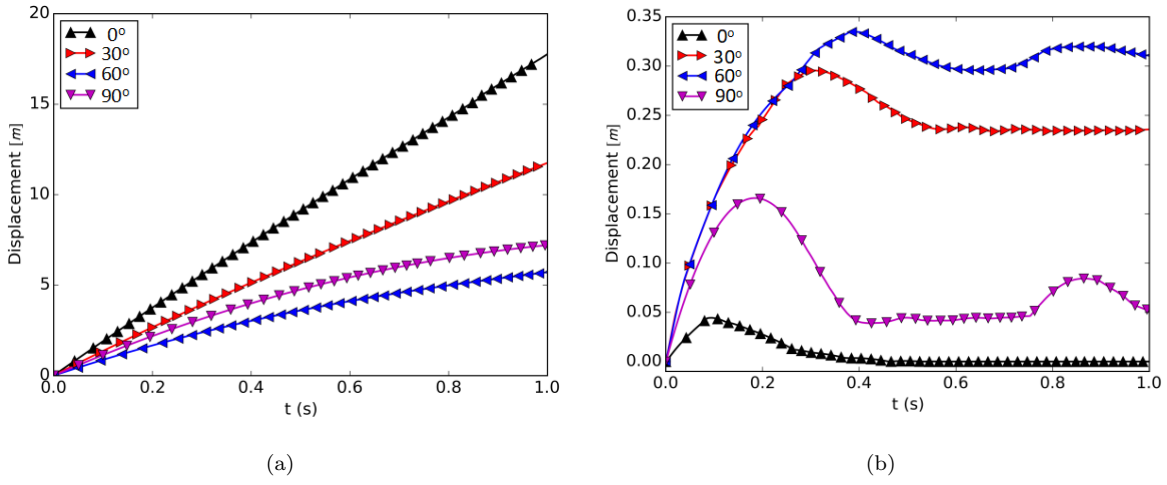


Figure 16: The displacement of (a) ice block and (b) marked ballast for different angles in longitudinal section

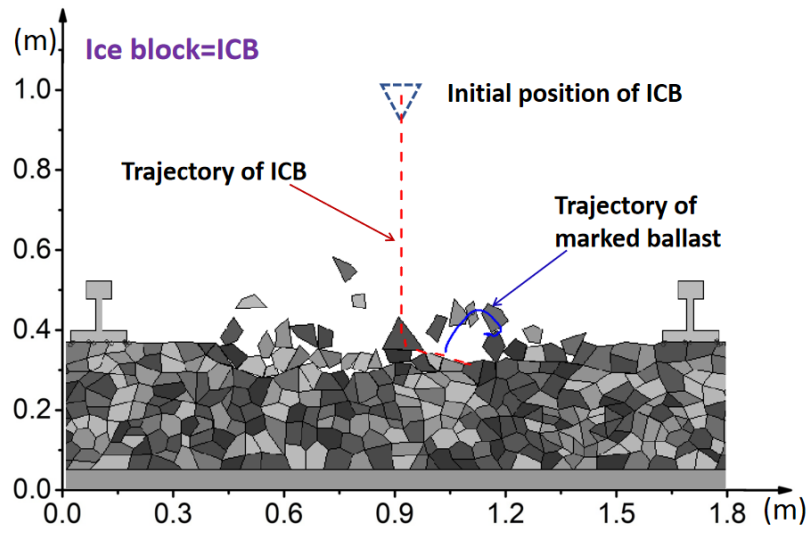
causes the maximum displacement of ballast particles, followed by the circular ice and then the square ice.

An investigation by the Japan Railway Technical Research Institute showed that the density of the packing snow and ice at the bottom of a train is from  $150$  to  $900 \text{ kg/m}^3$  and the maximum weight of snow / ice that may drop is about  $15 \text{ kg}$ . Furthermore, the shape of the snow / ice block which drops from the train is various and irregular [27]. Therefore, the ballast flight caused by different shapes of snow / ice block is very complex and serious.

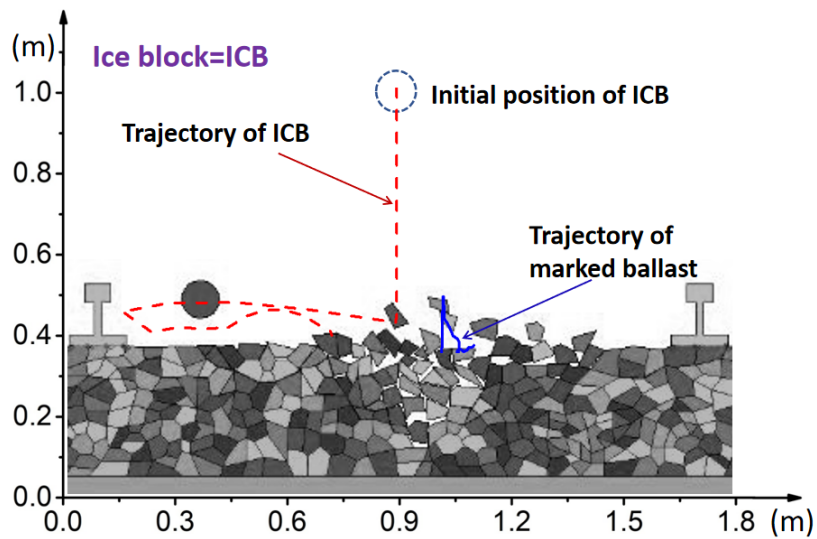
## 5. Conclusions

A numerical model based on the discontinuous deformation analysis (DDA) method, was proposed to study the dynamic behavior of ballast stones and their collision with a snow / ice block. This study took into account the shapes of the ice blocks and the contacts between ballast particles, where we assumed that contact constraints were imposed through the penalty method. The ballast flight induced by the dropping snow / ice with some variations in intensity depends on the velocity, the incident angle, and shapes of the ice blocks. The main findings derived from the numerical simulation may be summarized as follows:

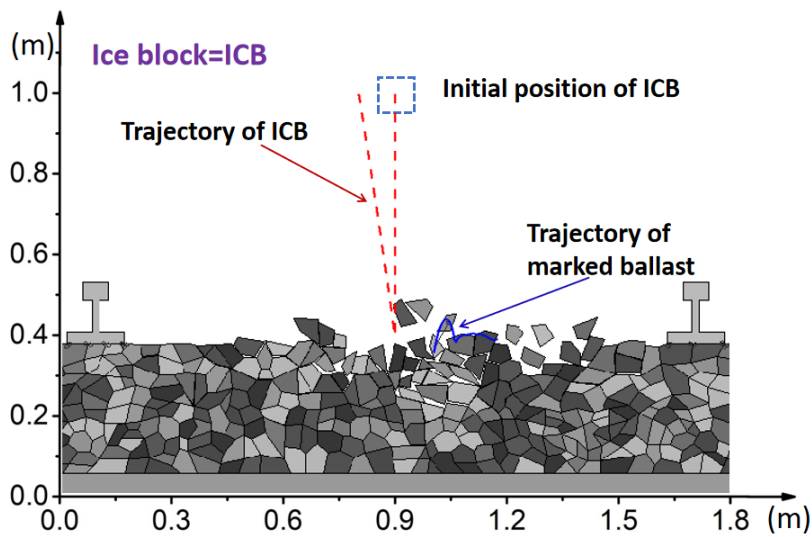
- The velocity of the snow / ice block, which directly depends on the running speed of the train and the position of the ice attached, has a great impact on the ballast flight. In the longitudinal-section, the number of flying ballast particles and their displacement increases from  $100 \text{ km/h}$  to  $400 \text{ km/h}$ . When the longitudinal velocity of the ice block is in the range of  $200 \text{ km/h}$  to  $300 \text{ km/h}$ , the results exhibit a peak of 33 % and 47 % of the total number of flying ballast and maximum of flying height of marked ballast. When the dropping longitudinal velocity is more than  $300 \text{ km/h}$ , the marked ballast may collide with the train underframe since the maximum height of the marked ballast after the collision is more than  $330 \text{ mm}$ . Hence, setting the maximum operating speed according to the weather conditions is an effective measure to reduce serious consequences.
- The angle of impact greatly influences the direction of the movement of the ballast particles. The angle of incoming snow / ice blocks, which indeed are the impacting projectiles, is closely related to



(a)



(b)



(c)

Figure 17: Relationship between ballast flight and ice block shape: (a) Triangle; (b) Circle; (c) Square

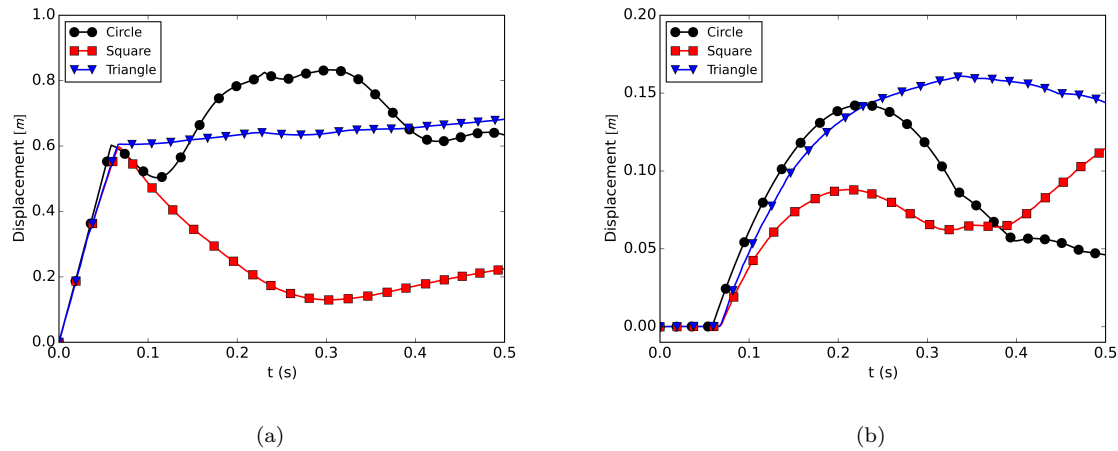


Figure 18: The displacement of (a) ice block and (b) marked ballast of different shapes

the location of a detaching projectile. Hence, it is worthwhile that, in order to significantly reduce the  
 270 ballast flight caused by the melting of snow / ice blocks, some measures should be taken to prevent  
 snow accumulating in the train and snow settlement.

- The shape of the snow / ice block affects the extent of ballast flight. The triangular ice block intrudes  
 the ballast bed directly after collision, while the square ice bounces off. The triangular ice ejects the  
 greatest number of particles and caused the greatest height of ejection. The square ice has the widest  
 275 and the deepest impact among the three.

Also, it is worth noting that very little research has been done on ice block and ballast particle breakage  
 from the point of view of aerodynamic interactions and numerical modeling . The breakage process is very  
 important as it may indicate the violence of the impact after the flying ballast collision step. Thus, the  
 analysis of the breakage process by the DDA method is still an open problem which should be undertaken  
 280 in future studies.

## Acknowledgements

The study is supported by the China Scholarship Council.

## References

- [1] A. Quinn, M. Hayward, C. Baker, F. Schmid, J. Priest, W. Powrie, A full-scale experimental and  
 285 modelling study of ballast flight under high-speed trains, *Journal of Rail and Rapid Transit* 224 (2)(2010)  
 61–74.
- [2] A. Sanz-Andres, F. Navarro-Medina, The initiation of rotational motion of a lying object caused by  
 wind gusts, *Journal of Wind Engineering and Industrial Aerodynamics* 98 (12) (2010) 772–783.

- [3] A. Premoli, D. Rocchi, P. Schito, C. Somaschini, G. Tomasini, Ballast flight under high-speed trains: Wind tunnel full-scale experimental tests, *Journal of Wind Engineering and Industrial Aerodynamics* 145 (2015) 351–361.
- [4] M. R. Saat, F. B. Jacobini, E. Tutumluer, Identification of high-speed rail ballast flight risk factors and risk mitigation strategies., Tech. rep., U.S. Department of Transportation, Federal Railroad Administration, Office of Research and Development, Washington, DC 20590, Final report, No:DOT/FRA/ORD-15/03, 76 pages (2015).
- [5] T.-R. Loponen, P. Salmenperä, H. Luomala, A. Nurmikolu, Studies of snow-dropping from a train on a turnout due to dynamic excitations, *Journal of Cold Regions Engineering* 32 (2) (2018) 04018003.
- [6] K. Kawashima, S. Iikura, T. Endo, T. Fujii, Experimental studies on ballast-flying phenomenon caused by dropping of accreted snow/ice from high-speed trains, *Railway Technical Research Institute Report* 17 (8) (2003) 31–36.
- [7] A. Khayrullina, B. Blocken, W. Janssen, J. Straathof, CFD simulation of train aerodynamics: train-induced wind conditions at an underground railroad passenger platform, *Journal of wind engineering and industrial aerodynamics* 139 (2015) 100–110.
- [8] J. Zhu, Z. Hu, Flow between the train underbody and trackbed around the bogie area and its impact on ballast flight, *Journal of Wind Engineering and Industrial Aerodynamics* 166 (2017) 20–28.
- [9] C. Paz, E. Suárez, C. Gil, Numerical methodology for evaluating the effect of sleepers in the underbody flow of a high-speed train, *Journal of Wind Engineering and Industrial Aerodynamics* 167 (2017) 140–147.
- [10] F. Xie, J. Zhang, G. Gao, K. He, Y. Zhang, J. Wang, Study of snow accumulation on a high-speed train’s bogies based on the discrete phase model., *Journal of Applied Fluid Mechanics* 10 (6) 1729–1745.
- [11] G.-H. Shi, R. E. Goodman, Generalization of two-dimensional discontinuous deformation analysis for forward modelling, *International Journal for Numerical and Analytical Methods in Geomechanics* 13 (4) (1989) 359–380.
- [12] G.-H. Shi, Discontinuous deformation analysis: a new numerical model for the statics and dynamics of deformable block structures, *Engineering computations* 9 (2) (1992) 157–168.
- [13] T. Ishikawa, Y. Ohnishi, A. Namura, DDA applied to deformation analysis of coarse granular materials (ballast), *Proc. 2nd Int. Conf. on Analysis of Discontinuous Deformation*. Japan Institute of Systems Research: Kyoto, Japan (1997) 253–262.
- [14] S.-C. Ji, A. Ouahsine, H. Smaoui, P. Sergent, G.-Q. Jing, Impacts of ship movement on the sediment transport in shipping channel, *Journal of Hydrodynamics* 26 (5) (2014) 706–714.

- [15] F. Linde, A. Ouahsine, N. Huybrechts, P. Sergent, Three-dimensional numerical simulation of ship resistance in restricted waterways: Effect of ship sinkage and channel restriction, *Journal of Waterway, Port, Coastal, and Ocean Engineering* 143 (1) (2016) 06016003.
- [16] D. M. Doolin, N. Sitar, Time integration in discontinuous deformation analysis, *Journal of engineering mechanics* 130 (3) (2004) 249–258.
- [17] T. T. Khanh, A. Ouahsine, H. Naceur, K. El Wassifi, Assessment of ship manoeuvrability by using a coupling between a nonlinear transient manoeuvring model and mathematical programming techniques, *Journal of Hydrodynamics* 25 (5) (2013) 788–804.
- [18] S.-G. Cai, A. Ouahsine, J. Favier, Y. Hoarau, Moving immersed boundary method, *International Journal for Numerical Methods in Fluids* 85 (5) (2017) 288–323.
- [19] S. Kaidi, M. Rouainia, A. Ouahsine, Stability of breakwaters under hydrodynamic loading using a coupled DDA/FEM approach, *Ocean Engineering* 55 (2012) 62–70.
- [20] L. Jing, Formulation of discontinuous deformation analysis (DDA):an implicit discrete element model for block systems, *Engineering Geology* 49 (3-4) (1998) 371–381.
- [21] D. M. Doolin, N. Sitar, Displacement accuracy of discontinuous deformation analysis method applied to sliding block, *Journal of engineering mechanics* 128 (11) (2002) 1158–1168.
- [22] J. Petrovic, Review mechanical properties of ice and snow, *Journal of materials science* 38 (1) (2003) 1–6.
- [23] F. Okonta, Effect of grading category on the roundness of degraded and abraded railway quartzites, *Engineering geology* 193 (2015) 231–242.
- [24] B. Suhr, K. Six, Parametrisation of a DEM model for railway ballast under different load cases, *Granular matter* 19 (4) (2017) 64:1–16.
- [25] C. J. Cho, Y. Park, New monitoring technologies for overhead contact line at 400 km/h, *Engineering* 2 (3) (2016) 360–365.
- [26] G. Jing, D. Ding, X. Liu, High-speed railway ballast flight mechanism analysis and risk management—a literature review, *Construction and Building Materials* 223 (2019) 629–642.
- [27] D. Navikas, H. Sivilevičius, Modelling of snow cover thickness influence on the railway construction temperature regime under variable weather conditions, *Procedia Engineering journal* 187 (2017) 124–134.